RSC Advances

PAPER

View Article Online
View Journal | View Issue

Cite this: *RSC Adv.*, 2022, **12**, 10379

Synthesis of BINOL–xylose-conjugates as "Turn-off" fluorescent receptors for Fe^{3+} and secondary recognition of cysteine by their complexes†

Huizhen Wang, Yang Liu, Yafeng Zhang and Xiaoxia Sun *

Received 22nd December 2021
Accepted 29th March 2022

DOI: 10.1039/d1ra09255c

rsc.li/rsc-advances

A novel chiral fluorescence "turn-off" sensor was synthesised using the click reaction. The sensor was a BINOL–xylose derivative, modified at the 2-position and linked by 1,2,3-triazole. It was structurally characterized by ^{1}HNMR, ^{13}CNMR, ESI-MS and IR analysis. The selectivity of *R*-β-D-2 in methanol solution has been studied. Among the 19 transition metal ions, alkaline metal ions and alkaline earth metal ions studied, *R*-β-D-2 had a selective fluorescence quenching reaction for Fe^{3+}. The detection limit of *R*-β-D-2 for Fe^{3+} was 0.91 μmol L^{-1}. Complexation between *R*-β-D-2 and Fe^{3+} was investigated by ESI-MS and ^{1}HNMR. The stoichiometric ratio of *R*-β-D-2 was 1 : 1. In addition, the *R*-β-D-2–Fe^{3+} complex was titrated with 20 naturally occurring amino acids and Hcy with GSH. It was found that the complex *R*-β-D-2–Fe^{3+} had a secondary recognition effect on Cys by switching to fluorescence.

Introduction

Selective recognition of Fe^{3+} and amino acids is an important research area in chemistry, biology and the environment.[1] Fe^{3+} plays a vital role in cell metabolism, haemoglobin oxygen transport and other vital activities as an indispensable ion in organisms. The imbalance in Fe^{3+} content will destroy cell stability and result in various diseases such as anemia, cancer and liver diseases.[2–6] However, in recent years, because of the rapid development of industry, industrial wastewater that has not been treated in accordance with standard practice has seriously affected the environment and public health, especially heavy metal ions that exceed the standard.[7,8] Amongst them, heavy metal ions are not biodegradable and will accumulate indefinitely in the bodies of organisms, so they have a deadly impact on human life and health.[9,10] Amino acids, an essential part of life,[11] play a vital role in organisms. Thiolic amino acids, such as cysteine (Cys), homocysteine (Hcy) and glutathione (GSH), are not only crucial to many physiological processes but also widely used in agriculture and food industry.[12–16] In the agricultural and food industry, a large quantity of cysteine is consumed in animal feed and food additives.[17,18] To date, absorption spectroscopy,[19] chemical precipitation,[20] ion exchange[21] and other methods have been used for the detection of Fe^{3+} and other heavy metal ions. But these methods require complex and long-standing instrumentation, a large number of chemical reagents and may cause secondary pollution.[22] As a result, they are not suitable for the detection of heavy metal ions. Recognition of cysteine is still under study, but the techniques used in the research are unstable, expensive equipment, bulky samples and other shortcomings.[23–28] Therefore, the design of sensors for the detection of ions and biological molecules has attracted extensive attention.[29]

It has been reported that rhodamine,[30,31] BODIPY,[32] calixarene,[33,34] cyclodextrin[35] and their derivatives can effectively identify metal ions, but it has not been found that they can perform secondary recognition for amino acids. It is well known that triazole compounds are used as corrosion inhibitors of organic copper, among which 1,2,4-triazole compounds are the most prominent.[36,37] However, 1,2,3-triazole has a good metal affinity with metal surfaces and are more vulnerable to attack by corresponding chemical entities than 1,2,4-triazoles.[33,38,39] Therefore, in this study, a novel triazole fluorescence sensor is reported and characterized. It is found that it can be used as a primary sensor to recognize Fe^{3+}, and its iron ion complex can also be used as a secondary sensor to recognize cysteine (Cys).

Experimental

Reagents and instruments

All analytical solvents were distilled prior to use. The drugs used were provided by reagent suppliers or synthesized through our lab *via* known routes and used without deep purification. Reagents used for chiral synthesis were optically pure unless otherwise specified. All kinds of metal ions (0.1 M) were prepared for corresponding metal nitrate in deionized water, while K^{+}, Hg^{2+}, Mn^{2+} and Ba^{2+} were prepared with chloride solution. Unless otherwise stated, $FeCl_3$ was used as the Fe^{3+} source. ^{1}HNMR and ^{13}CNMR were measured by Bruker AM-

Jiangxi Key Laboratory of Organic Chemistry, Jiangxi Science and Technology Normal University, Nanchang, 330013, China. E-mail: sunxiaoxia77@126.com

† Electronic supplementary information (ESI) available. See DOI: 10.1039/d1ra09255c

400WB spectrometer with TMS as internal standard and chloroform-D, acetone-D_6 or MeCN-D_3 as solvent. Infrared spectrum was determined by L1600301 binary Fourier transform infrared spectrometer. Fluorescence emission spectra were determined by Hitachi F-4500 and Hitachi F-4700 fluorescence spectrometers unless otherwise noted. ESI-MS spectral data were determined by Bruker Amazon SL Ion Trap Mass Spectrometer.

Synthesis of *R*-β-D-1 probe

R-1 (0.16 g, 0.43 mmol) and 1-azide-2,3,4-triacetoxy-β-D-xylose (0.27 g, 0.90 mmol) was added to a 100 mL eggplant flask. The system was sealed and vacuumed several times and protected by argon gas. 3 mL tetrahydrofuran was added eggplant flask at 2 to 8 degrees Celsius, and the system was fully stirred to completely dissolve it. Then sodium ascorbate (0.13 g, 0.64 mmol) and copper sulfate anhydrate (0.068 g, 0.43 mmol) was dissolved in 5 mL deionized water, and the color changed to yellow after full mixing. When the mixed solution was added to the system, the color of the system was yellow at the beginning, and the color of the solution changed to bright yellow at about 1 h, and then to grass green. The reaction at room temperature was 11 h, and the raw material point disappeared through TLC monitoring. Ice deionized water was added to the system to quench the reaction, then the crude product required was extracted with EA (ethyl acetate) for three times, and washed with saturated salt for one time, and dried with anhydrous Na_2SO_4 for 30 min. Using a circulating water pump to remove sodium sulfate, 200–300 mesh silica was added to the filtrate, and the solvent was dried through a rotary evaporator. Using petroleum ether and ethyl acetate as the eluent (v (petroleum ether) : v (ethyl acetate) = 4 : 1) for column chromatography, 0.39 g white solid was obtained with a yield of 90.6%. ^{1}HNMR (400 MHz, $CDCl_3$) δ 8.01 (d, J = 9.0 Hz, 2H), 7.94 (d, J = 8.1 Hz, 2H), 7.51 (d, J = 9.0 Hz, 2H), 7.40 (t, J = 7.3 Hz, 2H), 7.29–7.21 (m, 3H), 7.16 (d, J = 8.3 Hz, 2H), 6.91 (s, 2H), 5.61 (d, J = 9.1 Hz, 2H), 5.36 (t, J = 9.4 Hz, 2H), 5.19 (s, 6H), 4.22 (dd, J = 11.6, 5.6 Hz, 2H), 4.12 (q, J = 7.1 Hz, 1H), 3.54 (t, J = 11.0 Hz, 2H), 2.09 (d, J = 10.7 Hz, 12H), 1.75 (s, 6H). ^{13}CNMR (101 MHz, $CDCl_3$) δ 169.9, 168.7, 153.6, 134.1, 129.7, 128.1, 126.8, 125.6, 124.2, 120.6, 115.7, 86.2, 72.2, 70.8, 68.5, 65.4, 63.6, 20.8, 20.1 (ppm). MS (ESI$^-$): calcd for $[C_{48}H_{48}N_6O_{16}–H]^-$ 965.32; found 964.31.

Synthesis of *R*-β-D-2 probe

The synthesis process of *R*-β-D-2 was similar to that of *R*-β-D-1, so it will not be described much (details are in ESI†). The obtained *R*-β-D-2 was a white solid with a yield of 92%. ^{1}HNMR (400 MHz, MeOH-D_4) δ 7.99 (d, J = 9.0 Hz, 1H), 7.90 (s, 1H), 7.87 (d, J = 9.2 Hz, 2H), 7.54 (d, J = 9.0 Hz, 1H), 7.37 (s, 1H), 7.35–7.31 (m, 1H), 7.31–7.27 (m, 1H), 7.27–7.24 (m, 1H), 7.22 (d, J = 6.9 Hz, 1H), 7.15 (t, J = 8.3 Hz, 2H), 6.90 (d, J = 8.5 Hz, 1H), 5.84 (d, J = 9.0 Hz, 1H), 5.43 (t, J = 9.4 Hz, 1H), 5.26 (t, J = 9.2 Hz, 1H), 5.17 (s, 3H), 4.59 (s, 1H), 4.19 (dd, J = 11.4, 5.6 Hz, 1H), 3.69 (t, J = 11.0 Hz, 1H), 2.06 (s, 3H), 2.01 (s, 3H), 1.65 (s, 3H). ^{13}CNMR (101 MHz, $CDCl_3$) δ 170.0, 169.9, 169.0, 153.9, 151.8, 134.5, 134.2, 130.5, 130.0, 129.8, 129.3, 128.3, 128.1, 127.3, 126.7, 125.2, 125.0, 124.5, 123.5, 121.6, 118.2, 117.5, 115.5, 115.3, 86.6, 71.9, 70.7, 68.7, 65.9, 62.4, 20.8 (ppm). MS (ESI$^-$): calcd for $[C_{34}H_{31}N_3O_9–Na]^-$ 648.19; found 625.20.

Results and discussion

As shown in Scheme 1, 2,2′-position and 2-position modified BINOL–xylose derivatives *R*-β-D-1 and *R*-β-D-2 were synthesized by the easily procurable (*R*)-2,2′-bis (*O*-propargyloxymethyl)-1,1′-binaphthol (*R*-1) and (*R*)-2-(*O*-propargyloxymethyl)-1,1′-binaphthol (*R*-2). According to previous literature, NaH and K_2CO_3 were used as hydrogen pulling reagents of (*R*)-BINOL, then 3-bromo-1-propyne and (*R*)-BINOL after hydrogen pulling were used as reactants to obtain (*R*)-2,2′-bis (*O*-propargyloxymethyl)-1,1′-binaphthol (*R*-1) and (*R*)-2-(*O*-propargyloxymethyl)-1,1′-binaphthol with yields of 76% and 77%. Under the catalysis of anhydrous cupric sulfate and sodium ascorbate, the clicking reactions of 1-azide-2,3,4-triacetoxy-β-D-xylose and *R*-1 and *R*-2 were carried out in THF. The target sensors *R*-β-D-1 and *R*-β-D-2 with high yield were obtained. The structure of the target product was confirmed by IR, ^{1}HNMR, ^{13}CNMR and ESI-MS.

Fluorescence study

The fluorescence responses of *R*-β-D-1 (20 μM) and *R*-β-D-2 (20 μM) in methanol solvent under UV/visible light irradiation had been studied by fluorescence spectrometry. The absolute fluorescence quantum yield of *R*-β-D-2 was valued to be 0.079. As was shown in Fig. 1a, *R*-β-D-1 showed medium fluorescence at 385 nm (λ_{ex} = 300 nm). Different metal ions (including Fe^{2+}, Ca^{2+}, Ba^{2+}, Mn^{2+}, K^+, Sr^{2+}, Co^{3+}, Al^{3+}, Cr^{3+}, Mg^{2+}, Zn^{2+}, Ag^+, Hg^{2+},

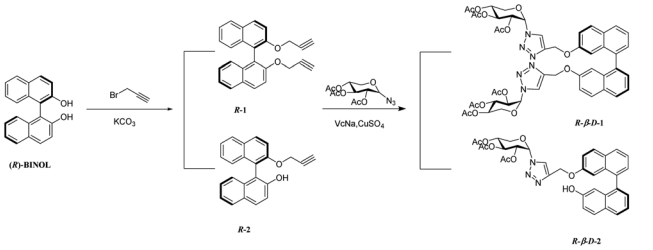

Scheme 1 Synthetic route for compounds *R*-β-D-1 and *R*-β-D-2.

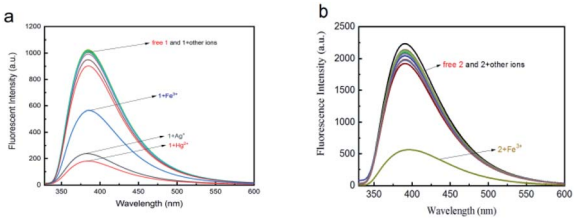

Fig. 1 Fluorescence spectra of (a) (*R*-β-D-1) and (b) (*R*-β-D-2) (20 μM in CH_3OH) in presence of various ions such as Fe^{2+}, Ca^{2+}, Ba^{2+}, Mn^{2+}, K^+, Sr^{2+}, Co^{3+}, Al^{3+}, Cr^{3+}, Mg^{2+}, Zn^{2+}, Ag^+, Hg^{2+}, Fe^{3+}, Pb^{2+}, Sn^{2+}, Cd^{2+}, Ni^{2+} and Cu^{2+} ions ((a) 1 + 5 equiv. ions, (b) 2 + 10 equiv. ions).

Fe^{3+}, Pb^{2+}, Sn^{2+}, Cd^{2+}, Ni^{2+} and Cu^{2+} ions) in methanol solution were recorded by the same fluorescence spectrometer. It was found that *R*-β-D-1 could simultaneously detect Fe^{3+}, Ag^{+}, and Hg^{2+}, and could not identify only one ion. However, as displayed in Fig. 1b, *R*-β-D-2 also had a moderate intensity of fluorescence at 390 nm (λ_{ex} = 318 nm) in methanol solution. It was found that *R*-β-D-2 had an obvious fluorescence quenching phenomenon for Fe^{3+} in the fluorescence response of different ions by fluorescence spectrometer. Except for Fe^{3+}, no other metal ions revealed significant quenching fluorescence emission intensity under 318 nm excitation, which proved that *R*-β-D-2 could specifically recognize Fe^{3+}. At the same time, after the addition of Fe^{3+}, the color of the detection solution changed from colorless to yellow, and its characteristic color change indicated that the naked eye detection of Fe^{3+} was feasible. These results indicated that *R*-β-D-2 could be used as Fe^{3+} fluorescence probe in methanol solution and had a high selectivity and sensitivity. The fluorescence quenching of Fe^{3+} after addition of *R*-β-D-2 might be due to the intramolecular proton transfer of the excited phenolic hydroxyl group to the adjacent OCH_2 group through the transition state, and the metal ion chelation might be due to the photoinduced electron transfer (PET effect). The results showed that the nitrogen atoms of the 1,2,3-triazole unit and the oxygen atoms of BINOL provided binding sites for metal ions on *R*-β-D-2.

Metal ion competition studies. For purpose of farther verify the high selectivity of fluorescence probe *R*-β-D-2 for Fe^{3+}, the competitive experiment was carried through as indicated in Fig. 2. The fluorescence emission intensity was detected at 390 nm *via* mixing other different metal ions (10.0 equiv.) with Fe^{3+} ions of the same equivalent. The results indicated that other coordination metal ions had little interference on the fluorescence intensity of *R*-β-D-2–Fe^{3+}. This signified that *R*-β-D-2 could be used as a specific sensor in the presence of background competing ions.

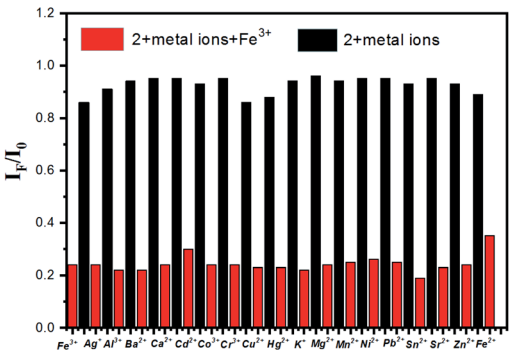

Fig. 2 Fluorescence quenching degrees I_F/I_0 of 1 (20 μM) valued at 390 nm in the presence of both Fe^{3+} (10.0 equiv.) and competing metal ions (10.0 equiv.). Black bars delegate the addition of 10 equiv. of a variety of metal ions to the solution of *R*-β-D-2 (20 μM in CH_3OH); red bars delegate the addition of the competing metal ions added to the existence of Fe^{3+}. I_0 states the fluorescence intensity of only *R*-β-D-2 and I_F states the fluorescence intensity with the addition of the commixture of competitive metal ions and Fe^{3+}.

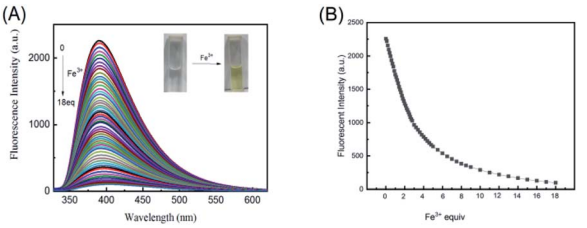

Fig. 3 (A) Fluorescence responses of *R*-β-D-2 (20 μM in CH_3OH, λ_{ex} = 318 nm) in the presence of increasing amount 0–18 equiv. Fe^{3+} (0.01 M). (B) The change of fluorescence intensity at 390 nm upon various equiv. Fe^{3+}.

The investigation of mechanism. The fluorescence response of *R*-β-D-2 to different concentrations of Fe^{3+} was also measured at room temperature, as indicated in Fig. 3. On the basis of the titration, when the concentration of Fe^{3+} increased from 0 to 18.0 equiv., the fluorescence intensity at 390 nm gradually decreased, and when the concentration of Fe^{3+} was 18.0 equiv., the fluorescence intensity dropped to the lowest point. There was a satisfactory linear relationship between the highest fluorescence intensity and the concentration of Fe^{3+}.

For the purpose of determining the adhesion between *R*-β-D-2 and Fe^{3+}, graph of Job's plot was plotted in MeOH by the methods that had been reported. The overall concentration of *R*-β-D-2 and Fe^{3+} was 2.0×10^{-5} M. As shown in Fig. 4(A), the molar fraction of [Fe^{3+}] reached its maximum value when the molar fraction of [Fe^{3+}]/([*R*-β-D-2] + [Fe^{3+}]) was about 0.5, indicating that BINOL–xylose compound was bonded to Fe^{3+} in the form of 1 + 1 complex. The result of this work (Fig. 4(B)) directly demonstrated that 1 : 1 was the stoichiometric ratio of the newly formed complex. According to the relation diagram of $I_0/(I_0 - I)$ and 1/[Fe^{3+}], the association constant (K_a) of *R*-β-D-2 and Fe^{3+} was

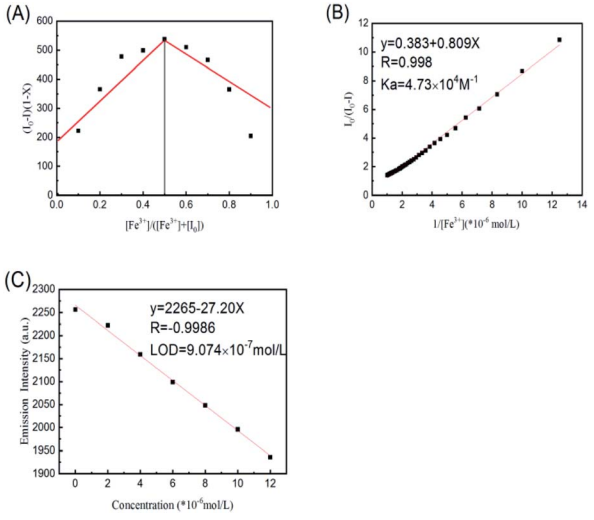

Fig. 4 (A) The job plot of a 1 : 1 complex of *R*-β-D-2 with Fe^{3+}. X was the molar fraction of Fe^{3+}. (B) Hildebrand–Benesi plot of $I_0/(I_0 - I)$ *versus* 1/[Fe^{3+}] based on the 1 : 1 binding stoichiometry. The binding constant K_a was calculated to be 4.73×10^4 M^{-1}. (C) LOD = 9.074×10^{-7} mol L^{-1}.

calculated by Hildebrand–Benesi equation as 4.73×10^4 M^{-1} ($R = 0.998$). Based on "LOD = $3\sigma/s$", the detection limit of a new type of sensor *R*-β-D-2 towards Fe^{3+} was calculated to be 9.074×10^{-7} M by fluorescence titration experiment with varying Fe^{3+} concentration (Fig. 4(C)). Compared with the known reports, this probe still had high sensitivity.[40]

Another evidence for 1 : 1 stoichiometric formation of complexes was determined from ESI-MS spectral data (Fig. 5). A significant free *R*-β-D-2 molecular ion peak was obtained at $m/z = 648.1944$ provided by $[R\text{-β-D-2} + Na^+]^+$. A new peak was observed at $m/z = 685.4375$ due to the fact that the complex *R*-β-D-2–Fe^{3+} lost a H_3O^+ and seized a Na^+ ($[(R\text{-β-D-2–}Fe^{3+}) + Na^+ – H_3O^+]$, $m/z = 685.11$). This result was in favor of our assumption that the formed *R*-β-D-2–Fe^{3+} complex had a strong adhesion with iron(III) ions. The binding mechanism of *R*-β-D-2 and Fe^{3+} was shown in Scheme 2.

In order to further research the complexation mechanism, ^{1}HNMR titration experiment was carried out in CD_3CN, as depicted in Fig. 6, to chase down more specific combination information between Fe^{3+} and *R*-β-D-2. According to Fe^{3+} equivalent (from 0 to 0.24), the chemical displacement of Fe^{3+} was obviously moved to the high field region. When Fe^{3+} was added into the sensor solution, the H_a of 6.64 ppm phenolic hydroxyl group disappeared completely, indicating that the oxygen atoms and Fe^{3+} in the phenolic hydroxyl group were related to the coordination of *R*-β-D-2. However, the proton H_b on the 1,2,3-triazole ring showed a significant upward shift, $\Delta\delta = 0.13$ ppm, from 7.48 ppm to 7.35 ppm, revealing that iron(III) ion combined with nitrogen-atoms on the triazole ring.

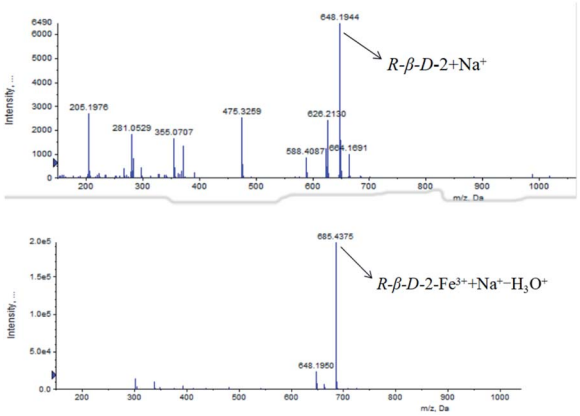

Fig. 5 ESI-MS spectral changes of *R*-β-D-2 and *R*-β-D-2–Fe^{3+}.

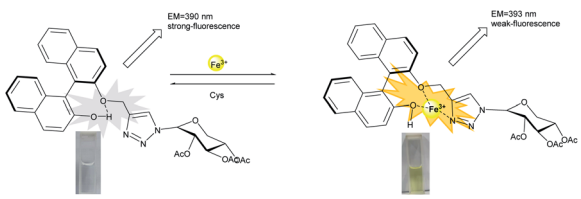

Scheme 2 Fluorescence-switching behaviors of *R*-β-D-2 induced by Fe^{3+}/Cys.

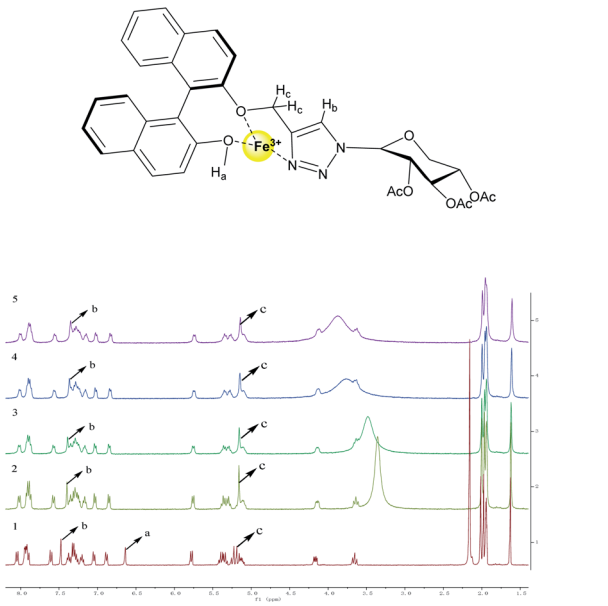

Fig. 6 ^{1}HNMR spectra of (1) *R*-β-D-2; (2) addition of 0.06 equiv. of Fe^{3+}; (3) addition of 0.12 equiv. of Fe^{3+}; (4) addition of 0.18 equiv. of Fe^{3+}; (5) addition of 0.24 equiv. of Fe^{3+}.

The NMR peak H_c, $–OCH_2–$, which connected the 1,2,3-triazolium groups, revealed a weak front-field shift from 5.19 ppm to 5.14 ppm. The results proved that Fe^{3+} was selectively coordinated with $–OCH_2–$ and triazole ring. The results of mass spectrometry, fluorescence titration and nuclear magnetic resonance spectroscopy proved that BINOL–xylose derivative formed a 1 : 1 binding mode with Fe^{3+}.

Fluorescence and absorption titrations of [Fe^{3+}–(*R*-β-D-2)] by amino acids. After the fluorescence detection of *R*-β-D-2, the complex *R*-β-D-2–Fe^{3+} (20 μM in CH_3OH, 10 equiv. Fe^{3+}) was used as a novel sensor for the secondary recognition of amino acids. As shown in Fig. 7(A), fluorescence of *R*-β-D-2–Fe^{3+} was enhanced at 393 nm in the presence of cysteine (Cys). And other amino acids (including GSH, Trp, His, Ile, Phe, Lys, Ser, Met, Ala, Arg, Leu, Val, Gly, Asn, Gln, Pro, Asp, Thr, Glu, Tyr, Hcy and Cys) did not show fluorescence enhancement, which proved that *R*-β-D-2–Fe^{3+} could specifically recognize Cys. In order to further validate the high selectivity of *R*-β-D-2–Fe^{3+} for Cys, as revealed in Fig. 7(B), a competitive experiment was carried out. Fluorescence emission intensity was measured at 393 nm by mixing other different amino acids of 10.0 equiv. with equivalent Cys. The results showed that other amino acids had little interference with the fluorescence intensity of *R*-β-D-2–Fe^{3+}–Cys. This meant that the sensor *R*-β-D-2–Fe^{3+} could be used as a specific sensor to detect background competitive amino acids. Meanwhile, as directed in Fig. 8, the color of the detected solution changed from yellow to colorless after the addition of Cys. Fluorescence enhancement was observed at 393 nm during the titration of *R*-β-D-2–Fe^{3+} by Cys, which was the opposite of what occurs when *R*-β-D-2 was titrated by Fe^{3+}, suggesting that Cys removed Fe^{3+} and thus released free *R*-β-D-2.

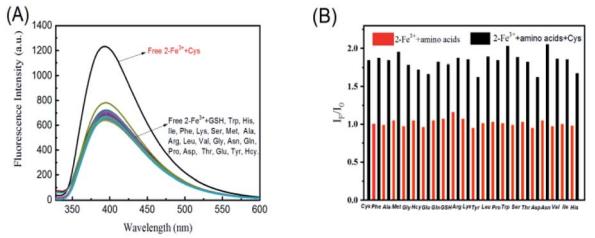

Fig. 7 (A) Fluorescence spectra of *R*-β-D-2–Fe^{3+} (20 μM in CH_3OH, 10 equiv. Fe^{3+}) in the presence of various amino acids such as GSH, Trp, His, Ile, Phe, Lys, Ser, Met, Ala, Arg, Leu, Val, Gly, Asn, Gln, Pro, Asp, Thr, Glu, Tyr, Hcy and Cys (10 equiv. amino acids). (B) Fluorescence enhancing degrees I_F/I_0 of 1 (20 μM) valued at 393 nm in the presence of both Cys (10.0 equiv.) and competing amino acids (10.0 equiv.). Red bars represent the addition of 10 equiv. of various amino acids to the solution of *R*-β-D-2–Fe^{3+} (20 μM in CH_3OH, 10 equiv. Fe^{3+}); black bars represent the addition of the competing amino acids added to the existence of Cys. I_0 states the fluorescence intensity of only *R*-β-D-2–Fe^{3+} and I_F states the fluorescence intensity with the addition of the mixture of competing amino acids and Cys.

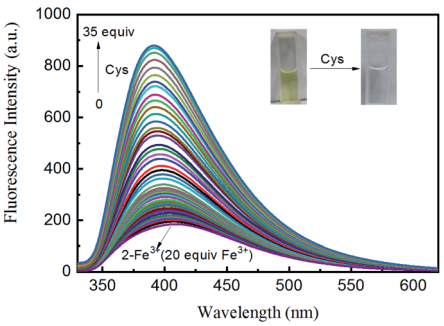

Fig. 8 Fluorescence responses of *R*-β-D-2–Fe^{3+} (20 μM in CH_3OH, 20 equiv. Fe^{3+}, λ_{ex} = 318 nm) in the presence of increasing amount 0–35 equiv. Cys (0.01 M).

In order to further determine the release of *R*-β-D-2 and the complexation of Fe^{3+} by Cys, *R*-β-D-2–Fe^{3+} and cysteine were detected by mass spectrometry, as shown in Fig. 9. ESI-MS showed that the main peak was free $[R\text{-β-D-2} + Na^+]^+$ (m/z = 648.1980), which clearly demonstrated that Cys removed Fe^{3+} and thus released *R*-β-D-2.

According to the above characteristics, a logical cycle was carried out for *R*-β-D-2, Fe^{3+} and Cys, as shown in Fig. 10. The figure indicated the reversibility of sensor *R*-β-D-2 in the

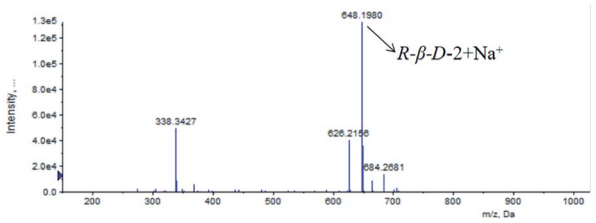

Fig. 9 ESI-MS spectral changes of *R*-β-D-2–Fe^{3+} and Cys.

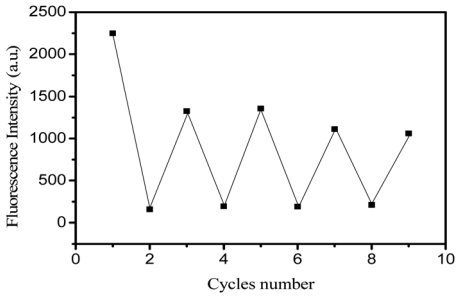

Fig. 10 The fluorescence reversibility of *R*-β-D-2 (0.04 μM) in CH_3OH solution between Fe^{3+} (20–38–55–75 equiv.) and cysteine (50–95–145–155 equiv.) at 390 nm.

presence of different concentrations of Fe^{3+} and cysteine. After four cycles, the sensor still worked well, indicating that *R*-β-D-2 was a highly reversible probe for sensing Fe^{3+} and cysteine.

Conclusions

A BINOL-based xylose derivative of 1,2,3-triazole was designed and synthesized *via* the click reaction of 1-azide-2,3,4-triacetoxy-β-D-xylose with (*R*)-BINOL chromophore, and its characterization was further carried out. The metal ions recognition performance of xylose derivatives at 2,2′-position and 2-position was extensively explored by spectroscopic techniques. Among the 19 different metal ions studied, the derivative *R*-β-D-1 could not specifically recognize a single metal ion in methanol solution. On the contrary, the derivative *R*-β-D-2 showed a selective fluorescence shutdown response to Fe^{3+}.

Through the fluorescence recognition response of *R*-β-D-1 and *R*-β-D-2 to different metal ions and the competitive experiment and fluorescence titration of *R*-β-D-2 to Fe^{3+}, the high sensitivity and selectivity of *R*-β-D-2 in Fe^{3+} sensing and almost free from the interference of coordination metal ions were confirmed. The formation, stoichiometry and binding modes of the complex were determined by fluorescence emission spectrophotometry, ESI-MS and ^{1}HNMR studies, and the formation of the complex was determined to be 1 : 1. The fluorescence quenching induced by Fe^{3+} was attributed to intramolecular proton transfer of the excited phenolic hydroxyl group to the adjacent OCH_2 group through a transition state form and metal ion chelation of photoinduced electron transfer (PET effect). Moreover, according to the results of this paper, nitrogen atoms of 1,2,3-triazole unit and oxygen atoms of BINOL provided binding sites for metal ions on *R*-β-D-2.

The secondary detection amino acids of *R*-β-D-2–Fe^{3+} complexes were further explored. Through the interaction of –SH side chain functional groups, selective fluorescence on reaction for Cys was produced in 20 naturally occurring amino acids and Hcy and GSH, thus making *R*-β-D-2 and its Fe^{3+} complex system interesting. Titration of Cys by *R*-β-D-2–Fe^{3+} and ESI-MS results showed that Fe^{3+} was displaced from the binding site of *R*-β-D-2 complex after adding Cys. Based on these results, the enhanced logic gate was constructed and it was found that the sensor *R*-β-D-2 still worked well after many cycles, indicating

that *R*-β-D-2 was a highly reversible probe for sensing Fe^{3+} and cysteine.

Conflicts of interest

There are no conflicts to declare.

Acknowledgements

The authors are grateful for the financial support of the National Natural Science Foundation of China (No. 21462018), the Science Fund of the Technology Office of Jiangxi, China (20192BAB203003) and Jiangxi Science and Technology Normal University Program for Graduate Innovation Fund (YC2020-X21).

Notes and references

1 J. Dessingou, A. Mitra, K. Tabbasum, G. S. Baghel and C. P. Rao, Benzimidazole conjugate of 1,1′-thiobis(2-naphthol) as switch-On fluorescence receptor for Ag^{+} and the complex as secondary recognition ensemble toward Cys, Asp, and Glu in aqueous methanolic solution: Synthesis, characterization, ion and amino acid recognition, computational studies, and microscopy features, *J. Org. Chem.*, 2012, **77**, 371–378.

2 M. W. Hentze, M. U. Muckenthaler, B. Galy and C. Camaschella, Two to tango: Regulation of mammalian iron metabolism, *Cell*, 2010, **142**, 24–38.

3 T. A. Rouault, The role of iron regulatory proteins in mammalian iron homeostasis and disease, *Nat. Chem. Biol.*, 2006, **2**, 406–414.

4 B. F. Shi, Y. B. Su, L. L. Zhang, M. J. Huang, R. J. Liu and S. L. Zhao, Nitrogen and phosphorus co-doped carbon nanodots as a novel fluorescent probe for highly sensitive detection of Fe^{3+} in human serum and living cells, *ACS Appl. Mater. Interfaces*, 2016, **8**, 10717–10725.

5 N. Narayanaswamy and T. Govindaraju, Aldazine-based colorimetric sensors for Cu^{2+} and Fe^{3+}, *Sens. Actuators, B*, 2012, **161**, 304–310.

6 S. X. Wang, X. M. Meng and M. Z. Zhu, A naked-eye rhodamine-based fluorescent probe for Fe(III) and its application in living cells, *Tetrahedron Lett.*, 2011, **52**, 2840–2843.

7 Y. Han, X. Wu, X. Zhang, Z. Zhou and C. Lu, Dual functional biocomposites based on polydopamine modified cellulose nanocrystal for Fe^{3+}-pollutant detecting and autoblocking, *ACS Sustainable Chem. Eng.*, 2016, **4**, 5667–5673.

8 Y. Wu, H. Pang, Y. Liu, X. Wang, S. Yu, D. Fu, J. Chen and X. Wang, Environmental remediation of heavy metal ions by novel-nanomaterials: A review, *Environ. Pollut.*, 2019, **246**, 608–620.

9 G. Aragay, J. Pons and A. Merkoci, Recent trends in macro-, micro-, and nanomaterial-based tools and strategies for heavy-metal detection, *Chem. Rev.*, 2011, **111**(5), 3433–3458.

10 S. Dong, W. Ji, Z. Ma, Z. Zhu, N. Ding, J. Nie and B. Du, Thermosensitive fluorescent microgels for selective and sensitive detection of Fe^{3+} and Mn^{2+} in aqueous solutions, *ACS Appl. Polym. Mater.*, 2020, **2**, 3621–3631.

11 Y. Y. Zhu, X. D. Wu, S. X. Gu and L. Pu, Free amino acid recognition: A bisbinaphthyl-based fluorescent probe with high enantioselectivity, *J. Am. Chem. Soc.*, 2019, **141**, 175–181.

12 H. L. Wang, G. D. Zhou and X. Q. Chen, An iminofluorescein-Cu^{2+} ensemble probe for selective detection of thiols, *Sens. Actuators, B*, 2013, **176**, 698–703.

13 J. B. Schulz, J. Lindenau, J. Seyfried and J. Dichgans, Glutathione, oxidative stress and neurodegeneration, *Eur. J. Biochem.*, 2000, **267**, 4904–4911.

14 S. Seshadri, A. J. Selhub, P. F. Jacques, I. H. Rosenberg, R. B. D'Agostino, P. W. F. Wilson and P. A. Wolf, Plasma homocysteine as a risk factor for dementia and alzheimer's disease, *N. Engl. J. Med.*, 2002, **346**, 476–483.

15 R. O. Ball, G. Courtney-Martin and P. B. Pencharz, The in vivo sparing of methionine by cysteine in sulfur amino acid requirements in animal models and adult humans, *J. Nutr.*, 2006, **136**, 1682S–1693S.

16 R. Hong, G. Han, J. M. Fernandez, B. J. Kim, N. S. Forbes and V. M. Rotello, Glutathione-mediated delivery and release using monolayer protected nanoparticle carriers, *J. Am. Chem. Soc.*, 2006, **128**, 1078–1079.

17 N. Kallscheuer, Engineered microorganisms for the production of food additives approved by the European Union-A systematic analysis, *Front. Microbiol.*, 2018, **9**, 1746.

18 H. Liu, Y. Wang, Y. H. Hou and Z. M. Li, Fitness of chassis cells and metabolic pathways for L-cysteine overproduction in Escherichia coli, *J. Agric. Food Chem.*, 2020, **68**, 14928–14937.

19 L. Suo, X. Dong, X. Gao, J. X. Huang, J. Ye and L. Zhao, Silica-coated magnetic graphene oxide nanocomposite based magnetic solid phase extraction of trace amounts of heavy metals in water samples prior to determination by inductively coupled plasma mass spectrometry, *Microchem. J.*, 2019, **149**, 104–112.

20 S. Mahdavi, M. Jalali and A. Afkhami, Heavy metals removal from aqueous solutions using TiO_2, MgO, and Al_2O_3 nanoparticles, *Chem. Eng. Commun.*, 2013, **200**, 448–470.

21 H. R. Fu, Z. X. Xu and J. Zhang, Water-stable metal-organic frameworks for fast and high dichromate trapping via single-crystal-to-single-crystal ion exchange, *Chem. Mat.*, 2015, **27**(1), 205–210.

22 J. Khan, M. Sadia, S. W. A. Shah, R. Naz and F. Ali, 2,6-bis(E)-(4-methylbenzylidine)-cyclohexan-1-one as a fluorescent-on sensor for ultra selective detection of chromium ion in aqueous media, *J. Fluoresc.*, 2021, **31**, 1759–1770.

23 M. H. Lee, J. S. Kim and J. L. Sessler, Small molecule-based ratiometric fluorescence probes for cations, anions, and biomolecules, *Chem. Soc. Rev.*, 2015, **44**, 4185–4191.

24 X. Dai, Z. Y. Wang, Z. F. Du, J. Cui, J. Y. Miao and B. X. Zhao, A colorimetric, ratiometric and water-soluble fluorescent probe for simultaneously sensing glutathione and cysteine/homocysteine, *Anal. Chim. Acta*, 2015, **900**, 103–110.

25 X. Kuang, S. Ye, X. Li, Y. Ma, C. Zhang and B. Tang, A new type of surface-enhanced Raman scattering sensor for the

enantioselective recognition of D/L-cysteine and D/L-asparagine based on a helically arranged Ag NPs@homochiral MOF, *Chem. Commun.*, 2016, **52**, 5432–5435.

26 H. Li, J. Fan, J. Wang, M. Tian, J. Du, S. Sun, P. Sun and X. Peng, A fluorescent chemodosimeter specific for cysteine: effective discrimination of cysteine from homocysteine, *Chem. Commun.*, 2009, 5904–5906.

27 M. S. Han and D. H. Kim, Rationally designed chromogenic chemosensor that detects cysteine in aqueous solution with remarkable selectivity, *Tetrahedron*, 2004, **60**, 11251–11257.

28 J. S. Shen, D. H. Li, M. B. Zhang, J. Zhou, H. Zhang and Y. B. Jiang, Metal-metal-interaction-facilitated coordination polymer as a sensing ensemble: A case study for cysteine sensing, *Langmuir*, 2011, **27**, 481–486.

29 G. X. Yin, Y. B. Gan, H. M. Jiang, T. Yu, M. L. Liu, Y. Y. Zhang, H. T. Li, P. Yin and S. Z. Yao, Direct quantification and visualization of homocysteine, cysteine, and glutathione in alzheimer's and parkinson's disease model tissues, *Anal. Chem.*, 2021, **93**(28), 9878–9886.

30 Y. Kim, G. Jang and T. S. Lee, New Fluorescent Metal-Ion Detection Using a Paper-Based Sensor Strip Containing Tethered Rhodamine Carbon Nanodots, *ACS Appl. Mater. Interfaces*, 2015, **7**, 15649–15657.

31 S. Panja, S. Mondal, S. Ghosh, U. Ghosh and K. Ghosh, Effect of substitution at amine functionality of 2,6-diaminopyridine-coupled rhodamine on metal-ion interaction and self-Assembly, *ACS Omega*, 2020, **5**(23), 13984–13993.

32 B. L. Sui, S. Tang, T. H. Liu, B. Kim and D. B. Kevin, Novel BODIPY-based fluorescence turn-on sensor for Fe^{3+} and its bioimaging application in living cells, *ACS Appl. Mater. Interfaces*, 2014, **6**, 18408–18412.

33 P. Sreedevi, J. B. Nair, P. Preethanuj, B. S. Jeeja, C. H. Suresh, K. K. Maiti and R. L. Varma, Calix[4]arene based redox sensitive molecular probe for sers guided recognition of labile iron pool in tumor cells, *Anal. Chem.*, 2018, **90**, 7148–7153.

34 V. S. Bieber, E. Ozcelik, H. J. Cox, C. J. Ottley, J. K. Ratan, M. Karaman and S. Badyal, Capture and release recyclable dimethylaminomethyl-calixarene functional cloths for point-of-use removal of highly toxic chromium water pollutants, *ACS Appl. Mater. Interfaces*, 2020, **12**(46), 52136–52145.

35 C. M. Singaravelu, X. Deschanels, C. Rey and J. Causse, Solid-state fluorescent carbon dots for fluorimetric sensing of Hg^{2+}, *ACS Appl. Nano Mater.*, 2021, **4**(6), 6386–6397.

36 J. L. Chen, X. H. Zeng, P. Ganesan, L. H. He, J. S. Liao, S. J. Liu, H. R. Wen, F. Zhao and Y. Chi, Heterobimetallic copper(i) complexes bearing both 1,1-bis(diphenylphosphino)ferrocene and functionalized 3-(2-pyridyl)-1,2,4-triazole, *New J. Chem.*, 2019, **43**, 4261–4271.

37 S. U. Ofoegbu, T. L. P. Galv∼ao, J. R. B. Gomes, *et al.*, Corrosion inhibition of copper in aqueous chloride solution by 1H-1,2,3-triazole and 1,2,4-triazole and their combinations: electrochemical, Raman and theoretical studies, *Phys. Chem. Chem. Phys.*, 2017, **19**(8), 6113–6129.

38 R. Balasubramanian, R. M. I. Fathima, P. Thirukumaran, *et al.*, Synthesis and properties of polytriazoleimide containing anthracene, pyridine and 1, 2, 3-triazole groups and their nanocomposites with titanium dioxide, *Polym. Eng. Sci.*, 2019, **59**(1), 129–138.

39 D. Urankar, B. Pinter, A. Pevec, F. De Proft, I. Turel and J. Kosmrlj, Click-triazole N2 coordination to transition-metal ions is assisted by a pendant pyridine substituent, *Inorg. Chem.*, 2010, **49**, 4820–4829.

40 G. Kumar, R. Guda, A. Husain, R. Bodapati and S. K. Das, A Functional Zn(II) Metallacycle Formed from an N-Heterocyclic Carbene Precursor: A Molecular Sensor for Selective Recognition of Fe^{3+} and IO^{4-} Ions, *Inorg. Chem.*, 2017, **56**, 5017–5025.